ELSEVIER

Contents lists available at ScienceDirect

Talanta

journal homepage: www.elsevier.com/locate/talanta



Boronic ester-functionalized dual-state emitter for oxygen/strain sensing and dynamic encryption

Weirao Ji ^{a,1}, Meiling Pan ^{b,1}, Jinyu Duan ^a, Lei Ma ^{b,c,d,*}, Yongtao Wang ^{a,**}

- ^a Guangxi Key Laboratory of Electrochemical and Magneto-Chemical Function Materia, College of Chemistry and Bioengineering, Guilin University of Technology, Guilin, 541004. China
- ^b Tianjin International Center for Nanoparticles and Nano System, Tianjin University, Tianjin, 300072, China
- ^c Haihe Laboratory for Low Dimensional Electronic Materials, Tianjin, 300074, China
- d Tianjin Key Laboratory of Low Dimensional Electronic Materials and Advanced Scientific Instrumentation, Tianjin, 300072, China

ARTICLE INFO

Keywords:

Room temperature phosphorescence Thermally activated delayed fluorescence Oxygen-detection Strain detection Host-guest doping

ABSTRACT

A novel luminogen named BTDA-BA was designed and synthesized, presenting simultaneously long-lived room temperature phosphorescence (RTP) and thermally activated delayed fluorescence (TADF) emissions in the glassy DMSO solution, rigid PMMA (polymethyl methacrylate) and PVA (polyvinyl alcohol), flexible PVC (polyvinyl chloride) and SIS (styrene-isoprene-styrene block copolymer) matrices. Noteworthy, RTP and TADF lifetimes of 1 % BTDA-BA@PVA film are up to 1307.28 ms and 566.55 ms in turn. Comparing four different doping matrices, BTDA-BA shows the best oxygen detection ability in PVC ($\lambda_{em} = 505$ nm, $\lambda_{ex} = 365$ nm), with high sensitivity to oxygen concentration changes, excellent reversibility, and good linear correlation between RTP intensity and oxygen concentration, whose detection range and K_{SV} are 0-2.1 × 10⁵ ppm and 1.96 × 10⁻⁵ ppm⁻¹, respectively. Besides, 1 % BTDA-BA@PVC film exhibits excellent strain-detection properties. By constructing ternary doping systems and utilizing Förster resonance energy transfer (FRET), long-lived orange afterglow is achieved. This work develops a novel dual-state long afterglow material, achieves persistent luminescence in both rigid and flexible matrices, and realizes efficient oxygen and strain detection, flexible displays, 3D modeling, and complex dynamic information encryption, which will contribute to boosting practical and theoretical advancements of multifunctional long afterglow materials.

1. Introduction

Thermally activated delayed fluorescence (TADF) and room temperature phosphorescence (RTP) are typically considered as two competing emissive processes [1–3]. Due to differing requirements of energy gap (ΔE_{ST}) between the lowest singlet (S1) and triplet (T1) states, developing pure organic materials simultaneously with TADF and RTP emissions faces a significant challenge [4,5]. Early research primarily focused on achieving efficient TADF or RTP materials individually [6]. With a deeper understanding of organic luminescence mechanisms, researchers have started to explore the coexistence and mutual conversion of TADF and RTP by molecular design and material engineering [7–10]. For instance, by introducing specific chemical groups, altering molecular structures, or employing host-guest doping strategies, some studies

have successfully observed the simultaneous presence of TADF and RTP [11]. Nevertheless, these materials often suffer from limitations such as short TADF and RTP lifetimes, low efficiencies, insufficient stability [12, 13]. Our research group has discovered a series of long-lived dual-band emission systems with TADF and RTP based on trace impurities in the synthesis process [14]. By adjusting the host-guest ratios, grinding, and materials temperature, these presented temperature-dependent dynamic afterglow. Subsequently, by altering the electronic effects of the substituent groups, the relationship between molecular structure and luminescent properties has been further explored [15,16]. However, when the guest molecules doped into rigid polymer matrices such as polyvinyl alcohol (PVA) and polymethyl methacrylate (PMMA), significantly shortened RTP and afterglow lifetimes were observed. Enhancing the dual-state emission performance of

^{*} Corresponding author. Tianjin International Center for Nanoparticles and Nano System, Tianjin University, Tianjin, 300072, China.

^{**} Corresponding author.

E-mail addresses: lei.ma@tju.edu.cn (L. Ma), wyt_shzu@163.com (Y. Wang).

 $^{^{1}}$ Contributed equally.

these guests in rigid and flexible polymer matrices would be of great theoretical and practical significance for boosting the practical applications of these materials and deep understanding of the luminescence mechanisms [17–20].

Host-guest doping strategy has emerged as a primary method for constructing efficient RTP materials [21-23]. By leveraging rigid host materials to restrict non-radiative transitions of guest molecules and optimizing excited state distributions via energy transfer between host and guest materials, phosphorescence efficiency and lifetime were enhanced and prolonged [24,25]. Even so, numerous challenges remain in developing flexible RTP materials [26-29]. Generally, most flexible matrices struggle to suppress molecular motions effectively, leading to increased non-radiative transitions of triplet excitons and consequently reducing phosphorescence lifetime and efficiency [30,31]. Currently, the applications of RTP materials are predominantly focused on anti-counterfeiting, where distinct afterglow colors and long lifetimes can be utilized to create highly secure and difficult-to-replicate identification marks [32-36]. However, the sensitivity of RTP materials to environmental factors, such as oxygen and moisture, limits their broader application in fields like bioimaging and sensing [37-42]. In the previous study, our research group employed PVC as a doping matrix to achieve strain detection. However, the corresponding RTP lifetime was short, with an afterglow lasting only 3 s [12]. To enhance RTP performance, the doping system needs further optimization by introducing highly efficient guest molecules. Oxygen molecules are potent quenchers of phosphorescence, making RTP materials highly sensitive to oxygen concentration [43]. By monitoring changes of phosphorescence intensity or lifetime, RTP materials can achieve high-sensitivity detection of oxygen levels. Additionally, long afterglow of RTP materials provides a unique advantage in time-resolved detection, effectively reducing background fluorescence interference [44]. However, to realize efficient oxygen sensing, specific requirements must be met by the doping matrix. Firstly, the matrix material should possess good oxygen permeability to allow rapid diffusion of oxygen into the phosphorescent material [45]. Secondly, it must protect the phosphorescent material from other environmental factors (such as moisture) while providing a stable luminescent environment [46]. Moreover, the matrix material should exhibit good mechanical properties and durability to adapt to various application environments [47]. In summary, although the host-guest doping strategy has achieved remarkable progress in constructing efficient RTP materials, substantial challenges persist in developing flexible RTP materials and expanding their application domains. Future research should focus on exploring and optimizing new doping systems to enhance RTP performance and stability, thereby unlocking the full potential of RTP materials in diverse applications [48].

The incorporation of boronic acid esters and boronic acid groups in RTP chromophores and doping systems has not only significantly enhanced phosphorescence efficiency and material stability but also provided new avenues for achieving stimulus responsiveness and multifunctional integration [49,50]. An et al. successfully fabricated a highly hydrolytically stable RTP film by forming crosslinked covalent bonds between boronic acid of luminogens and the hydroxyl groups of PVA, with RTP lifetimes of 3.18 s and RTP quantum yields of 11.33 % [51]. Li et al. developed a recyclable RTP material with high toughness and shape memory effects by using luminogens with boronic acid ester [52]. Li et al. obtained water and heat responsive RTP materials by arylboronic acids [53,54]. Based on the above reports and our laboratory's previous research results, a novel luminogen named BTDA-BA was designed and synthesized (Scheme S1). For comparison, BTDA, which has a similar molecular structure to BTDA-BA, was also prepared as a control (Scheme S1). By choosing various polymer matrices including rigid PVA and PMMA, as well as flexible polyvinyl chloride (PVC) and styrene-isobutylene-styrene block copolymer (SIS), a series of host-guest doping systems were constructed and optimized. The doping systems exhibited long-lived TADF and RTP. Specifically, TADF and RTP lifetimes of 1 % BTDA-BA@PVA film were 566.55 ms and 1307.28 ms,

respectively, with afterglow durations lasting up to 14.5 s. Oxygen detection experiments revealed that the 1 % BTDA@PVC film was highly sensitive to changes in oxygen concentration, with excellent reversibility and linear correlations between RTP intensity and oxygen concentration. Under uniaxial tensile testing, RTP emission intensity of the 1 % BTDA-BA@PVC film continuously decreases with increasing elongation, exhibiting strain-detection properties. Moreover, long-lived orange afterglow was achieved by constructing ternary doping systems and utilizing Förster resonance energy transfer (FRET). This work has also accomplished three-dimensional modeling and flexible displays, as well as dynamic information encryptions.

2. Experiment section

BTDA-BA was prepared by a two-step method. Detailed synthetic procedures, structural characterization, host-guest doping, and theoretical calculations are available in Supporting Information.

3. Results and discussion

As shown in Fig. 1a and Scheme S1, BTDA-BA and BTDA were designed and synthesized from 4-bromobenzaldehyde via a two-step synthetic approach, whose molecular structure and purity were characterized and confirmed by using ¹H NMR, ¹³C NMR, HR-MS, and HPLC (Fig. S1-8). BTDA-BA exhibited distinct absorption and emission behaviors across solvents, reflecting its electronic structure and solventpolarity-dependent interactions. In Tol, BTDA-BA exhibited two absorption bands, corresponding to π - π * transition of 280–330 nm and n- π * transition of 330-450 nm in turn (Fig. 1b). In contrast, three absorption bands (220-450 nm) emerged in the other three solvents, suggesting additional solvent-stabilized electronic states or charge-transfer contributions. With increasing solvent polarity from n-hexane to DMSO, the absorption maxima underwent a consistent red shift of 3-8 nm. Upon excitation at 365 nm, BTDA-BA displayed blue fluorescence in various solvents, with the emission maxima shifting by 17-50 nm towards longer wavelengths as solvent polarity increased (Fig. 1c). This solvatochromic effect confirms the presence of intramolecular charge transfer (ICT), where polar solvents stabilize the excited state more effectively than the ground state. To investigate the luminescent properties of BTDA-BA, phosphorescence spectra of BTDA-BA were measured at variable temperatures in dilute DMSO solution (Fig. 1d). At 77 K, a green afterglow (500 nm) dominated, characteristic of phosphorescence due to suppressed non-radiative decay in the rigid glassy matrix. Upon warming to 197 K, a new emission peak (420 nm) emerged, overlapping with fluorescence, suggesting coexistence of singlet and triplet pathways. At 227 K, the 450 nm peak intensified, confirming TADF, where reverse intersystem crossing (RISC) from triplets to singlets becomes efficient. At 287 K, the TADF emission plateaued, likely due to enhanced molecular motion quenching triplet excitons via non-radiative pathways. Based on fluorescence (437 nm) and delayed phosphorescence emission maxima (508 nm) of BTDA-BA in glassy DCM solution at 77 K (Fig. S9), ΔE_{ST} of BTDA-BA is 0.39 eV.

Polymer matrixes can provide a rigid environment for phosphorescent molecules, effectively suppressing non-radiative transitions and reducing quenching of triplet excitons by oxygen and water molecules through physical isolation. Additionally, polymers have excellent processability, allowing phosphorescent materials to be fabricated into films, fibers, or other shapes via solution processing and thermal forming, thereby facilitating large-scale production and flexible phosphorescent displays. However, factors such as the hydrogen-bonding capability of the polymer, interactions with the phosphorescent molecules (e.g., electrostatic forces, van der Waals forces), crystallinity, and compatibility with guests can all influence RTP and application performance of the doping systems, and these are difficult to predict accurately. Therefore, to optimize phosphorescence performance and enable efficient oxygen-detection, four polymers with different rigidities were

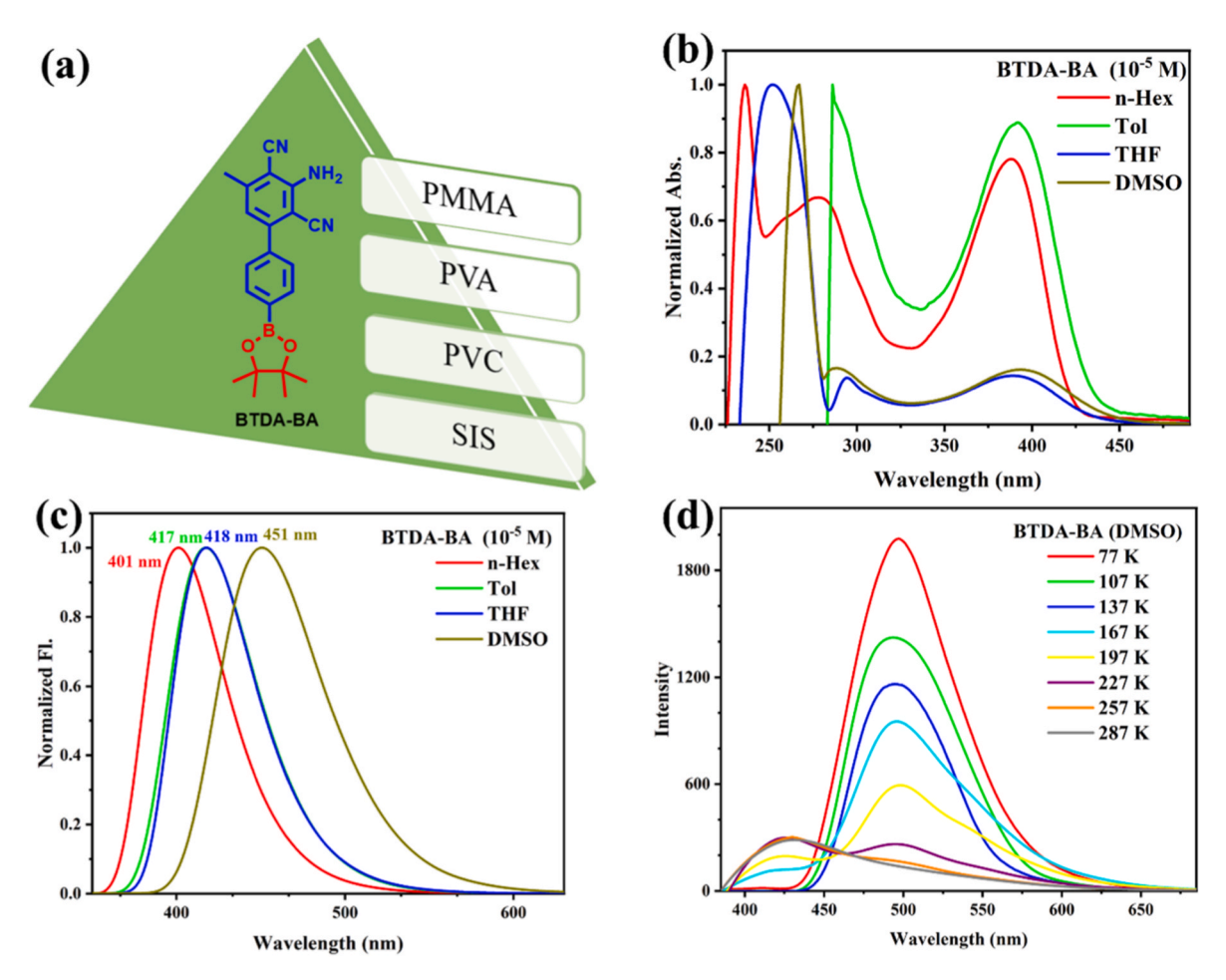


Fig. 1. (a) The molecular structure of BTDA-BA and four different doping matrices; (b)–(c) Normalized UV–vis absorption and fluorescence emission spectra of BTDA-BA in various solvents (λ_{ex} : 365 nm; solution concentration: 10^{-5} M); (d) Temperature-variable phosphorescence spectra of BTDA-BA in DMSO solution (τ_d : 0 ms, λ_{ex} : 365 nm).

chosen as doping matrices. A series of BTDA-BA-based doping systems were constructed using PMMA, PVA, PVC, and SIS as host materials, whose RTP performance was optimized by adjusting the doping mass ratio between BTDA-BA and hosts (Fig. S10-13). The doping systems were named according to host and guest materials, as well as their doping ratios. For example, 1 % BTDA-BA@PMMA film meant that BTDA-BA was doped into the PMMA matrix at a mass ratio of 1:100. Among different doping concentrations, 1 % BTDA-BA@PMMA, 1 % BTDA-BA@PVA, 1 % BTDA-BA@PVC, and 0.5 % BTDA-BA@SIS films exhibited the best RTP intensity and lifetime (Fig. S10-13). TADF and RTP emission maxima of four doping films were close to those in the glassy DMSO solution, which indicated that TADF and RTP of four doping systems originated from the monomolecular emission of BTDA-BA. In comparison, 1 % BTDA-BA@PVA film gave the longest afterglow duration (15 s), TADF and RTP lifetimes of 566.55 ms and 1307.28 ms in sequence, as well as RTP quantum yield (Φ_P) of 0.04 and ΔE_{ST} of 0.45 eV (Fig. 2 and Table 1), which should be attributed to the strong intermolecular hydrogen bonding and oxygen barrier effect of PVA, as well as good compatibility between PVA and BTDA-BA, leading to the smallest non-radiative phosphorescence rate (K_{nr}). The 1 % BTDA-BA@PMMA film followed, with afterglow duration of 8 s, TADF and RTP lifetimes of 832.71 ms and 580.23 ms, respectively, as well as Φ_P of 0.05 and ΔE_{ST} of 0.45 eV. Compared to rigid PVC and PMMA materials, PVC and SIS doping matrixes have better flexibility, which leads to increased molecular motions and reduced RTP lifetime. As a result, 1 % BTDA-BA@PVC and 0.5 % BTDA-BA@SIS films presented afterglow duration of 6 s and 7 s, TADF lifetimes of 542.57 ms and 288.70 ms, RTP

lifetimes of 674.46 ms and 705.08 ms in turn, corresponding to Φ_P of 0.05 and 0.02, ΔE_{ST} of 0.51 eV and 0.46 eV respectively. Furthermore, TADF and RTP emission characteristics of 1 % BTDA-BA@PMMA, 1 % BTDA-BA@PVC, and 0.5 % BTDA-BA@SIS films were confirmed by temperature dependent RTP spectra. Unlike the other three doping films, the TADF emission peak of the 1 % BTDA-BA@PVA film could not be detected when the delay time (τ_d) was 0 s, which may be due to a too low intensity ratio (I_{TADF}/I_{RTP}) between TADF and RTP. However, the TADF emission peak could be clearly captured when τ_{d} was increased to 3 ms (Fig. 2c). As τ_d was further extended from 3 ms to 50 ms, I_{TADF}/I_{RTP} continued to increase, which was attributed to a faster decay rate for RTP than TADF (Fig. 2e). Even so, the corresponding afterglow color changes were minimal when the emission spectra of 1 % BTDA-BA@PVA film at different delay times were plotted in the CIE chromaticity coordinates (Fig. 2f), which was consistent with the experimental observations. Of note, fluorescence emission maxima of the four doping films showed significantly red shifts compared to those of TADF at the same excitation wavelength, resulting in the reduced energy gaps $(\Delta E'_{ST})$ (Table 1). As a speculation, intermolecular interactions of BTDA-BA in doping films reduces the energy level of S₁ state, while TADF emission originates from BTDA-BA monomer. Furthermore, the main optical performance parameters were calculated and listed in Table 1. Compared with 1 % BTDA-BA@PMMA, 1 % BTDA-BA@PVC, and 1 % BTDA-BA@PVA films, 0.5 % BTDA-BA@SIS film had smaller $\Delta E'_{ST}$, resulting in increased TADF quantum yield (Φ_{TADF}). Furthermore, RTP performance of BTDA was also optimized by altering doping matrices and doping ratios (Fig. S14). By contrast, afterglow lifetime and

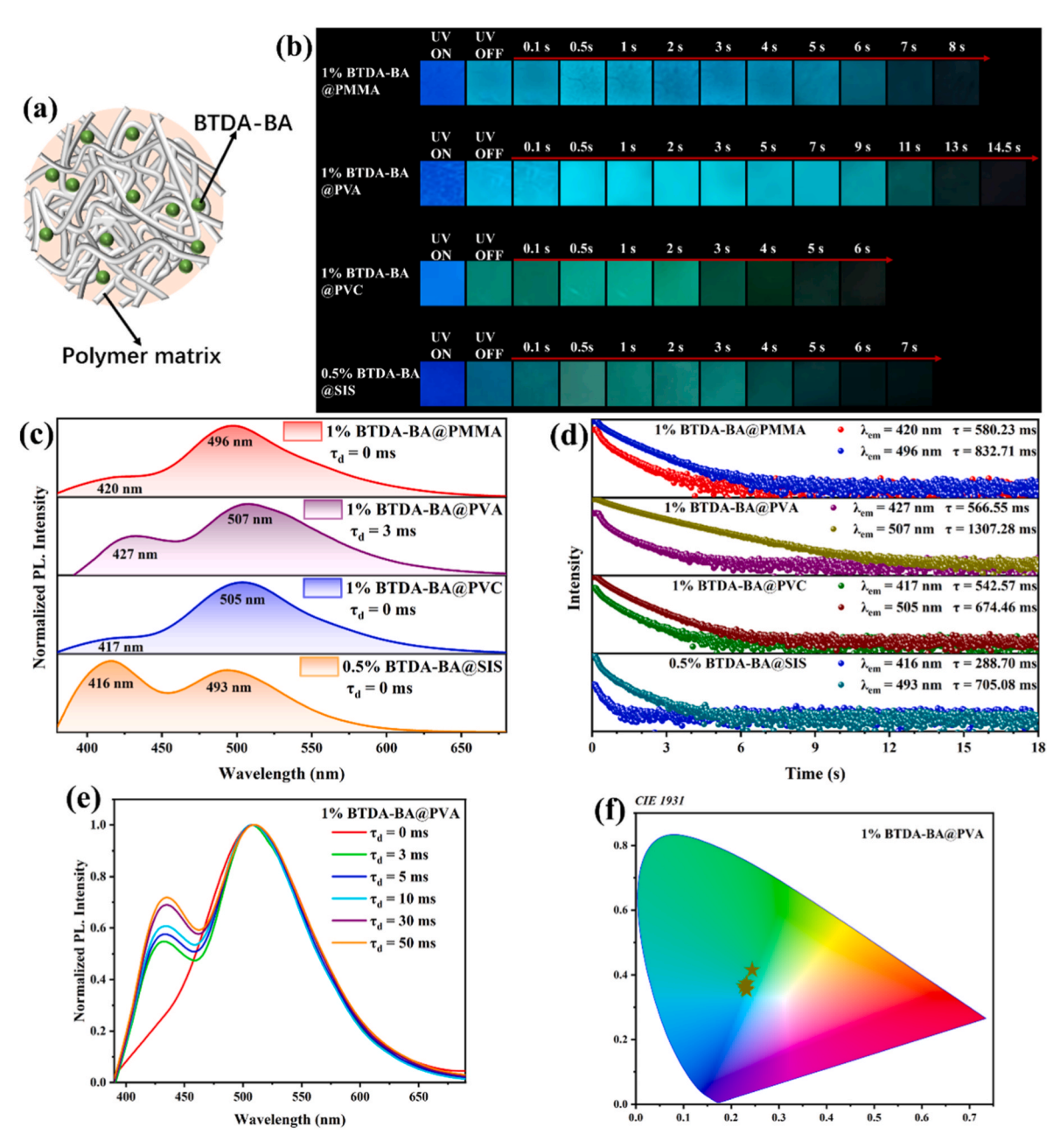


Fig. 2. (a) Schematic diagram of BTDA-BA@PVA and 0.5 % BTDA-BA@PVB and 0.5 % BTDA-BA@SIS films at different decay times (τ_d) (λ_{ex} : 365 nm); (d) The time-resolved phosphorescent decay curves of 1 % BTDA-BA@PWBA, 1 % BTDA-BA@PVB, 1 % BTDA-BA@PVB and 0.5 % BTDA-BA@PVB films at different τ_d : (e) Delayed RTP spectra of 1 % BTDA-BA@PVB film at different τ_d : (f) CIE chromaticity coordinates of 1 % BTDA-BA@PVB film at different τ_d .

Table 1 Photophysical properties of various films.

	λ _F (nm)	λ _P (nm)	τ _F (ns)	τ _{TADF} (ms)	τ_{P} (ms)	Φ _F (%)	Φ _{TADF} (%)	Φ _P (%)	K_{TADF} (s^{-1})	$K_{ISC} (10^8 s^{-1})$	(s^{-1})	K_{nr} (s^{-1})	ΔE_{ST} (eV)	$\Delta E'_{ST}$ (eV)
1	450	496	6.42	580.23	832.71	11.59	1.43	5.45	0.03	1.39	0.07	1.13	0.45	0.26
2	447	507	4.61	566.55	1307.28	4.56	1.26	4.49	0.02	2.07	0.04	0.72	0.46	0.33
3	453	505	5.34	542.57	674.46	3.95	0.92	5.06	0.02	1.80	0.08	1.40	0.52	0.28
4	452	493	4.56	288.70	705.08	8.16	1.66	1.79	0.06	2.01	0.03	1.39	0.47	0.23

 $[\]textcircled{3}: 1 \% \ BTDA-BA@PMMA; \ \textcircled{2}: 1 \% \ BTDA-BA@PVA; \ \textcircled{3}: 1 \% \ BTDA-BA@PVC; \ \textcircled{4}: 0.5 \% \ BTDA-BA@SIS$

 $[\]Delta E_{ST}$: The energy gap between TADF and RTP emission maxima.

 $[\]Delta E'_{ST}$: The energy gap between fluorescence and RTP emission maxima.

brightness of BTDA were significantly weaker than those of BTDA-BA in four doping matrixes, confirming the effectiveness of molecular design strategies of BTDA-BA. Especially, 1 % BTDA @PMMA and 0.5 % BTDA@SIS films did not present visible afterglow by switching on-off a 365 nm UV lamp. Noteworthy, the excellent RTP emission of BTDA-BA was closely related to intermolecular interactions of host and guest materials. Thereby, electrostatic interactions between BTDA-BA and four doping hosts were calculated, which showed that there were multiple intermolecular interactions between $-\mathrm{NH}_2$ and $-\mathrm{CN}$ of BTDA-BA and four doping matrixes (Fig. S15). For 1 % BTDA-BA@PVC and 0.5 % BTDA-BA@SIS films, borate ester group of BTDA-BA also formed obviously intermolecular interactions with PVC and SIS.

Oxygen can deactivate the triplet excitons of phosphorescent materials through energy transfer and collisional quenching. Therefore, RTP materials are theoretically suitable for oxygen detection. However, RTP materials usually have to be doped into polymer matrices to avoid rapid phosphorescence decay or quenching due to molecular motions. Notably, the polymer matrixes not only affect the RTP intensity and lifetime of RTP materials but also influence the oxygen detection performance. To evaluate the oxygen detection capabilities of phosphorescent materials in different doping matrices, various oxygen detection environments were constructed by adjusting the flow rates of air and oxygen using a gas flow controller. In comparison, the 1 % BTDA-BA@PVC film is more suitable for oxygen detection than the 1 % BTDA-BA@PMMA, 1 % BTDA-BA@PVA, and 0.5 % BTDA-BA@SIS films (Fig. 3 and Fig. S16). As shown in Fig. 3a and b, RTP intensity of 1 % BTDA-BA@PMMA and 1 % BTDA-BA@PVC films decreased gradually with increasing oxygen content from 0 % to 21 %. When the oxygen concentration reached 21 % (2.1 \times 10⁵ ppm), RTP intensity of 1 % BTDA-BA@PVC film at 505 nm was quenched 20.55-fold, while RTP intensity of 1 % BTDA-BA@PMMA film at 496 nm was only quenched 3.51-fold, indicating a higher oxygen quenching efficiency for 1 %

BTDA-BA@PVC film than 1 % BTDA-BA@PMMA film. The 1 % BTDA-BA@PVC film had a wide linear response range of oxygen concentrations from 0 to 2.1×10^5 ppm. Based on the Stern-Volmer relationship $I_0/I - 1 = K_{SV}$ [O₂], Stern-Volmer quenching plots for 1 % BTDA-BA@PVC film could be linearly fitted ($R^2 = 0.99155$), and the Stern-Volmer constant (K_{SV}) was calculated to be 1.96 \times 10⁻⁵ ppm. In contrast, Stern-Volmer quenching plots for 1 % BTDA-BA@PMMA film need to be fitted logarithmically ($R^2 = 0.9901$) instead of linearly, with a narrower linear range (0-1.05 \times 10⁵ ppm) (Fig. 3c), while 1 % BTDA-BA@PVA and 0.5 % BTDA-BA@SIS films show poor oxygen detection performance and fail to provide good linear relationship in Stern-Volmer quenching plots (Fig. S16). Compared with previously reported phosphorescent oxygen sensors, the 1 % BTDA-BA@PVC film has a wider linear response range and higher sensitivity, making it more advantageous for oxygen sensing applications (Table S2). To evaluate the reversible sensing capability towards oxygen, 1 % BTDA-BA@PVC film was alternately exposed to nitrogen and ambient air environments, whose phosphorescence intensity at 505 nm was monitored. The results indicated RTP intensity of the 1 % BTDA-BA@PVC film could be completely restored after repeating the cycle ten times (Fig. 3d). For 0.5 % BTDA-BA@SIS film, RTP intensity and oxygen content presented a logarithmic relationship, which could be non-linearly fitted, with a high correlation coefficient ($R^2 = 0.99353$). For 1 % BTDA-BA@PVA film, RTP intensity dropped rapidly when the oxygen concentration reached 7 % and above. Besides, neither 1 % BTDA-BA@PVA nor 0.5 % BTDA-BA@SIS films follow the Stern-Volmer relationship. Overall, the 1 % BTDA-BA@PVC film is most suitable for oxygen detection. To investigate the strain detection properties of the 1 % BTDA-BA@PVC film, a uniaxial tensile test was conducted based on the flexibility and stretchability of PVC matrix. Meanwhile, the relationship between the elongation and RTP performance was investigated. As shown in Fig. 3e and f, TADF and RTP emission intensities of the 1 % BTDA-BA@PVC film

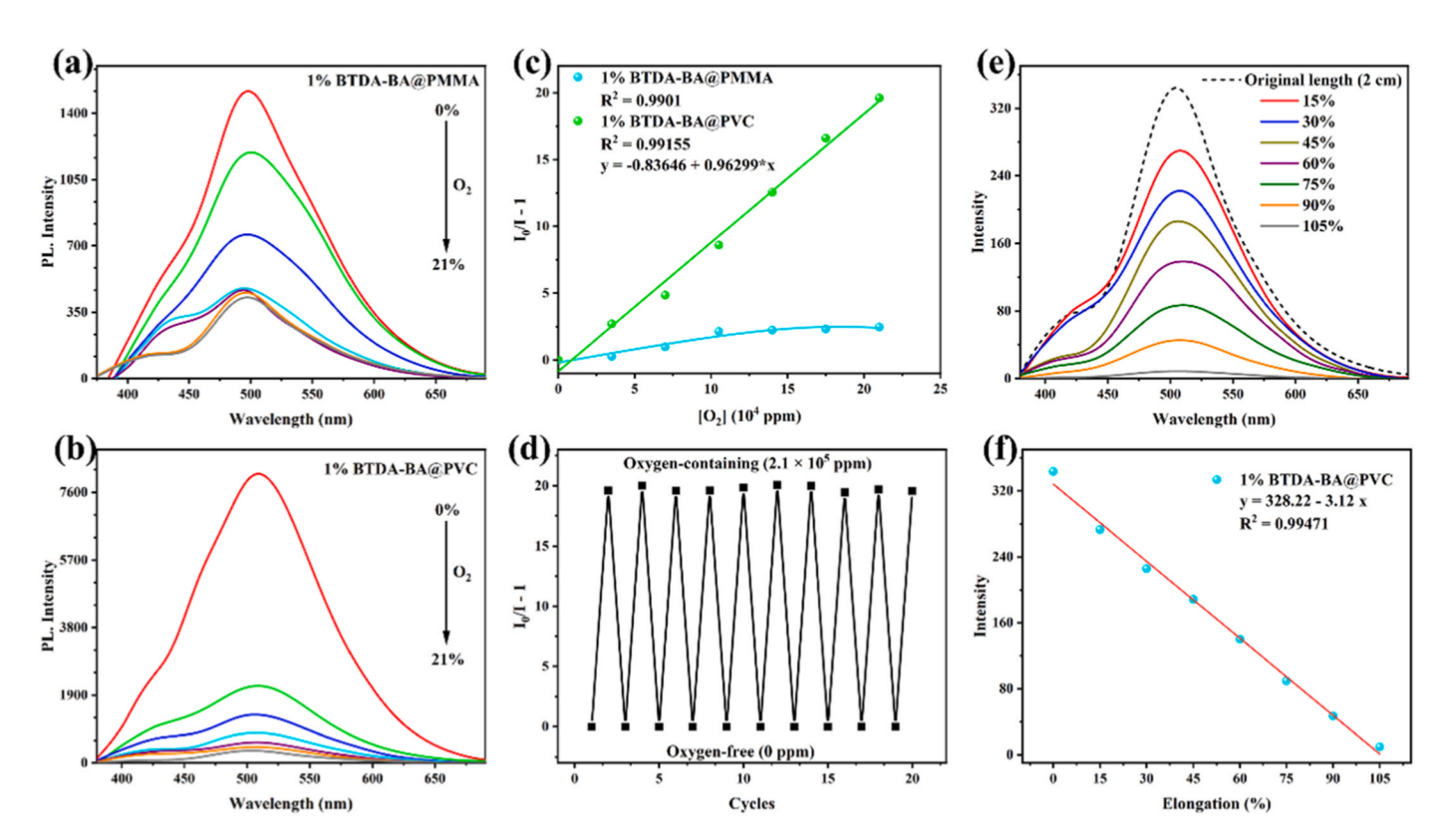


Fig. 3. (a)—(b) Phosphorescence spectra of the 1 % BTDA-BA@PMMA and 1 % BTDA-BA@PVC films at different oxygen concentrations; (c) Stern–Volmer quenching plots for 1 % BTDA-BA@PMMA and 1 % BTDA-BA@PVC films by oxygen; (d) Reversible oxygen response of 1 % BTDA-BA@PVC film; (e) Phosphorescence emission spectra of 1 % BTDA-BA@PVC film stretching from original length 0 % (2.0 cm) to 105 % (4.1 cm); (f) The variation tendency of RTP intensity of 1 % BTDA-BA@PVC film at different elongation.

gradually decreased with increasing elongation. Notably, the RTP emission intensity at 505 nm exhibited a strong linear correlation with the elongation (R² = 0.99471), whose linear fitting equation could be expressed as y = 328.22–3.12x, where y and x represent the RTP emission intensity and elongation in turn. The lowest detection limits (LOD) of 1 % BTDA-BA@PVC film for oxygen and strain are calculated using LOD = $3\sigma/k$, where σ is the standard deviation of the blank measurement and k is the slope of the RTP intensity vs oxygen concentration/elongation curve. The results show that the LOD of 1 % BTDA-BA@PVC film for oxygen and strain are 0.8896 ppm and 3.59 %, respectively (Fig. S17).

The geometric structures of BTDA-BA and BTDA were optimized at the B3LYP/def2-TZVP level of theory using D4 dispersion correction. Subsequently, single-point energy calculations were performed at the same B3LYP/def2-TZVP level. Thereby, the highest occupied molecular orbital (HOMO), the lowest unoccupied molecular orbital (LUMO), and electronic cloud density distribution of BTDA-BA and BTDA were obtained. Additionally, the spin-orbit coupling constants (ξ) between the singlet and triplet states were calculated (Fig. 4 and Fig. S18). As shown in Fig. 4a, HOMO of BTDA-BA is mainly concentrated on NH2 and the benzene ring of the dicyanobenzanilide structural unit, while LUMO is primarily distributed on -CN and ortho and meta carbon atoms of NH₂, with some distribution on the benzene bridge containing boronic ester group, exhibiting a significant ICT phenomenon, which is consistent with experimental results. In contrast, the HOMO and LUMO of BTDA are distributed throughout the entire molecule, showing electron shifts from the bromobenzene to the dicyanoaniline structural unit (Fig. S18). It can be concluded that replacing the bromine with a boronic ester group alters the distribution of HOMO and LUMO electron densities and ICT direction. Furthermore, BTDA-BA exhibits smaller HOMO-LUMO energy gaps compared with BTDA. Near S1 state of BTDA-BA, there are two triplet states (T_2 and T_3), corresponding to energy gaps and ξ of 0.29 eV, 0.366 cm⁻¹, 0.38 eV, and 0.071 cm⁻¹, respectively. In comparison, there are also two triplet states (T3 and T4) near the S1 state of BTDA, corresponding to smaller energy gaps (0.082 eV and 0.183 eV) and bigger ξ (1.627 cm⁻¹ and 0.460 cm⁻¹), confirming that BTDA is more prone to generating triplet excitons than BTDA-BA. However, the significantly increased ΔE_{ST} (1.53 eV), ΔE_{T1T2} (0.886 eV) and ΔE_{T1T3} (1.4452 eV) are not conducive to the formation of T₁ triplet excitons for BTDA (Fig. S18), leading to weaker RTP performance compared to AN-Br. At 77 K, phosphorescence and fluorescence spectra of BTDA-BA were determined in glassy CH₂Cl₂ solution, yielding ΔE_{ST} of 0.39 eV, which was indeed unfavorable for TADF emission. However, the coexistence of TADF and RTP was clearly shown based on the experimental results. Why does such a large ΔE_{ST} still allow for efficient TADF? Firstly, tripletriplet annihilation fluorescence was excluded based on TADF and RTP lifetimes. If it's triple-triplet annihilation mechanism, TADF lifetime should be half of RTP lifetime, which is inconsistent with the experimental results. Theoretical calculations reveal that the energy gap between S_1 and the second excited triplet state (T_2) is significantly smaller than ΔE_{ST} , which is likely the key reason underpinning the observed TADF. Furthermore, S_1 and T_2 states of BTDA-BA exhibit hybrid charge transfer states (HLCT), confirming that effective SOC and ISC can occur between S_1 and T_2 states (Fig. S19). Therefore, we attribute the origin of TADF emission to the small energy gap and big SOC between the S_1 and T_2 states.

Red and near-infrared (NIR) afterglow materials possess strong tissue penetration capabilities and minimal damage to biological tissues, making them highly promising for applications in bioimaging and biosensing. However, these materials often suffer from enhanced nonradiative energy losses, leading to deteriorated Φ_P and RTP lifetime. Recently, Förster resonance energy transfer (FRET) theory and the heavy-atom effect have played crucial roles in boosting red and NIR materials. Three ternary doping systems named RhB & BTDA-BA@PMMA, RhB & BTDA-BA@PVA, and RhB & BTDA-BA@PVC film were constructed by using BTDA-BA and Rhodamine B (RhB) as FRET donor and acceptor in sequence. The doping mass ratios of RhB, BTDA-BA, and PMMA/PVA/PVC were all set at 0.5:1:100. The results showed that the RhB & BTDA-BA@PVA film exhibited the longest afterglow duration (7 s) and the longest RTP lifetime (650.43 ms), with a maximum RTP peak at 586 nm (Fig. 5 and Fig. S20). The RhB & BTDA-BA@PMMA film followed, with afterglow durations of 5 s, RTP lifetimes of 500.48 ms, and RTP emission maxima at 591 nm. The RhB & BTDA-BA@PVC film gave the longest RTP emission maxima (597 nm), corresponding to RTP lifetimes and afterglow durations of 440.90 ms and 4 s, respectively (Fig. S20). By contrast, the RhB & BTDA-BA@PVA film showed the highest FRET efficiency (42.42 %) and the brightest afterglow(Table S1 and Fig. 5), which can be attributed to the optimal overlap between the RTP emission spectrum of 1 % BTDA-BA@PVA film and the UV-vis absorption spectrum of 0.5 % RhB@PVA film, while the afterglows of the RhB & BTDA-BA@PMMA and RhB & BTDA-BA@PVC films were relatively weaker due to the poor overlap. Overall, all three doping films presented dynamic afterglow behaviors, which can be ascribed to the relatively low FRET efficiency and the significant FRET differences between TADF and RTP efficiencies.

As shown in Fig. 6a, a square piece of 1 % BTDA-BA@PVC film was repeatedly folded, rolled, and twisted to create a three-dimensional (3D) rabbit model under ambient conditions. Subsequently, 1 % BTDA-BA@PVC film was cut into the shape of the Chinese character "朱" and then rolled. Turning on-off a 365 nm UV lamp, the 3D model and

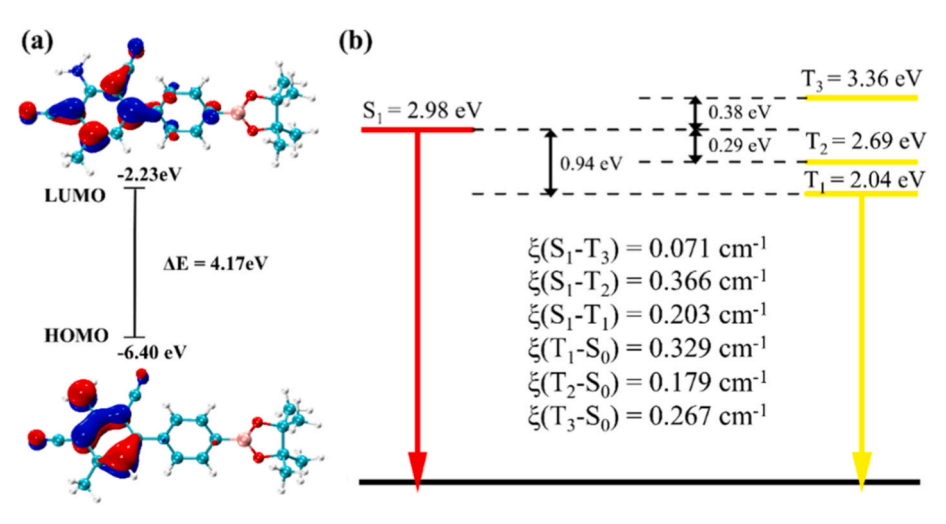


Fig. 4. (a) HOMO and LUMO distribution of BTDA-BA; (b) Energy levels and spin orbit coupling constants (ξ) of BTDA-BA.

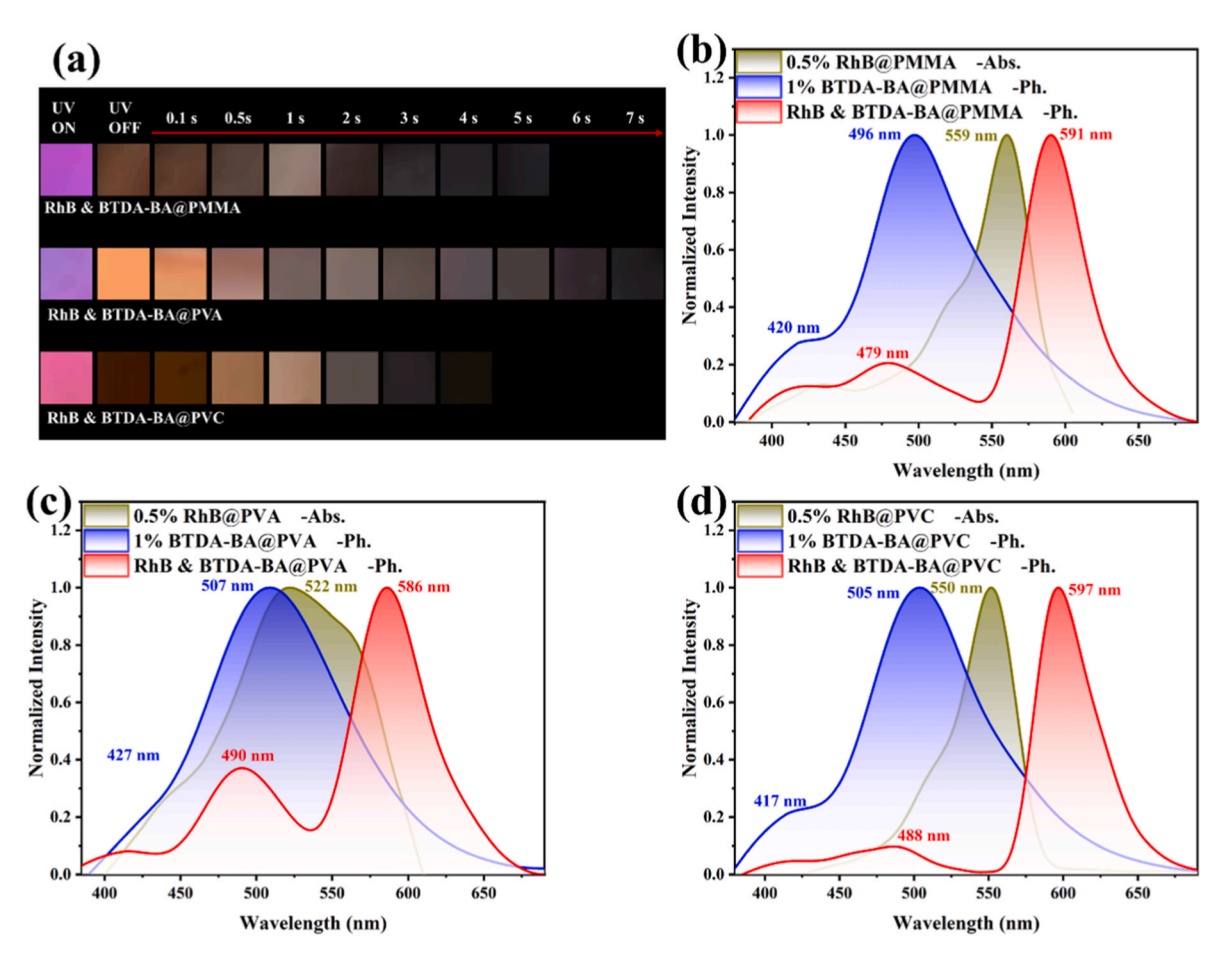


Fig. 5. (a) Photographs of RhB & BTDA-BA@PMMA, RhB & BTDA-BA@PVA and RhB & BTDA-BA@PVC films by turning on/off a 365 nm UV light lamp; (b)–(d) Normalized UV–vis absorption and fluorescence and phosphorescence emission spectra of RhB & BTDA-BA@PMMA, RhB & BTDA-BA@PVA and RhB & BTDA-BA@PVC films.

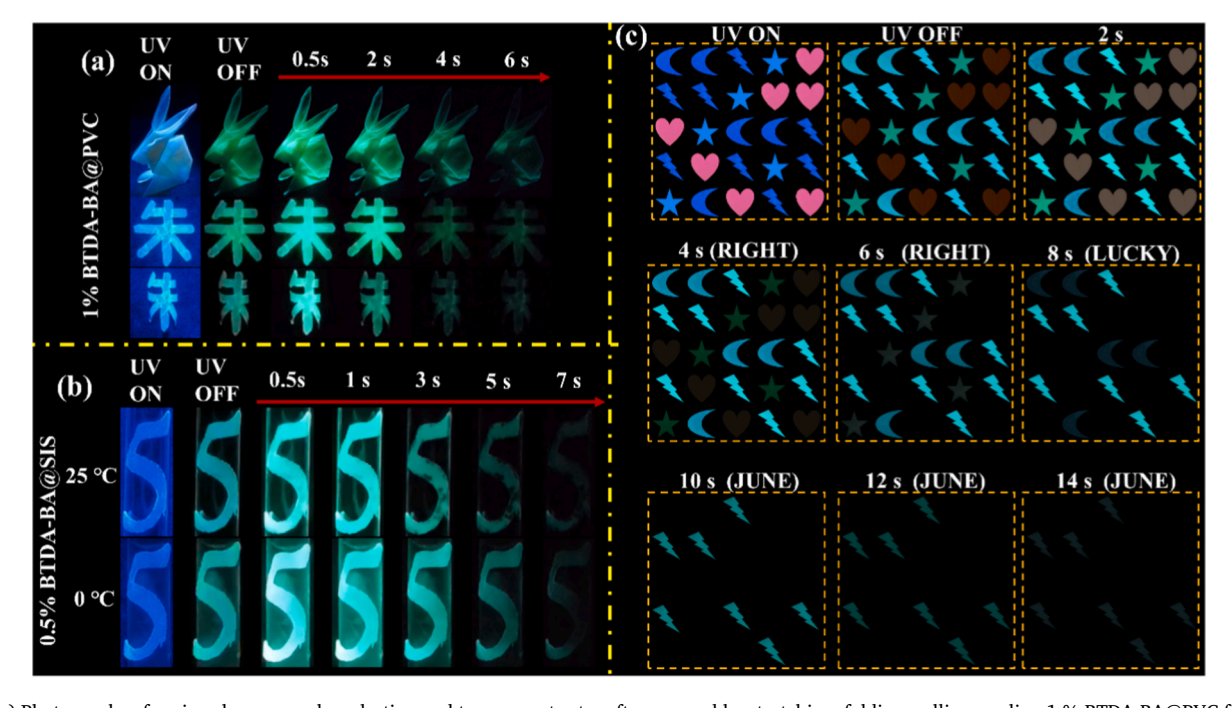


Fig. 6. (a) Photographs of various large area, long-lasting and transparent art crafts prepared by stretching, folding, rolling, curling 1 % BTDA-BA@PVC film under ambient conditions; (b) Photographs of stable transparent patterns prepared by rolling 0.5 % BTDA-BA@SIS film at different temperatures; (c) Information encryption by RhB & BTDA-BA@PVC, 1 % BTDA-BA@PMMA, 1 % BTDA-BA@PVC and 1 % BTDA-BA@PVA films.

Chinese character emitted bright blue-green afterglow lasting for 6 s, which was identical to the afterglow duration of the pristine 1 % BTDA-BA@PVC film. A piece of 0.5 % BTDA-BA@SIS film cut into the shape of the number "5" was rolled and attached to the surface of a transparent quartz tube. When the quartz tube was filled with H₂O and frozen to 273 K, the afterglow brightness of the number "5" slightly increased compared to that at room temperature, while the afterglow duration remained constant. Finally, RhB & BTDA-BA@PVC, 1 % BTDA-BA@PMMA, 1 % BTDA-BA@PVC, and 1 % BTDA-BA@PVA films were selected to form a series of heart, crescent, star, and lightning shapes, which were arranged in a 5×5 matrix. Based on unique arrangement patterns and colors, complex dynamic information encryptions were achieved (Fig. 6c). Referring to a specific codebook (Fig. S21), decryption was realized by turning on-off the 365 nm UV lamp. Under UV radiation, the matrix initially appeared to have no specific meaning. However, after turning off the UV lamp, the matrix could be decrypted to read "RIGHT" at 4-6 s, "LUCKY" at 8 s, and "JUNE" at 10 s.

4. Conclusion

In conclusion, a novel luminogen named BTDA-BA, containing a boronic ester group, was designed and synthesized, BTDA-BA shows simultaneously monomolecular TADF and RTP emissions in the glassy DMSO solution. By host-guest doping and optimization, BTDA-BA exhibits long-lived dual state emission not only in rigid matrices, but also in flexible doped matrices. Especially, 1 % BTDA-BA@PVA film gives RTP lifetime of 1307.28 ms, TADF lifetime of 566.55 ms, and afterglow durations of 14.5 s, which is rare in the reported dual state emission materials. Noteworthy, RTP lifetimes of 1 % BTDA-BA@PVC and 0.5 % BTDA-BA@SIS films are also up to 674.46 ms and 705.08 ms in turn, which are comparable to RTP lifetime of many chromophores in rigid matrices. Compared to rigid PVA and PMMA, BTDA-BA exhibited an increased K_{nr} in flexible PVC and SIS, resulting in shortened RTP lifetime and afterglow. Comparing four different doping matrices, 1 % BTDA@PVC film is the best oxygen detection material, with high sensitivity to oxygen concentration changes, excellent reversibility, and good linear correlation between RTP intensity and oxygen concentration, whose detection range and K_{SV} are 0–2.1 10^5 ppm and 1.96×10^{-5} ppm⁻¹, respectively. Meanwhile, 1 % BTDA-BA@PVC film exhibits excellent strain-detection properties, whose linear fitting equation between RTP emission intensity (v) and elongation (x) could be expressed as y = 328.22 - 3.12x. By contrast, the introduction of the boronic ester group significantly enhances RTP lifetime and brightness in various doping matrices due to the reduced energy gap (ΔE_{ST} and ΔE_{T1T2}) rather than increased intersystem transitions between singlet and triplet excitons, which minimizes non radiative energy loss. By constructing ternary doping systems and utilizing FRET, long-lived orange afterglow is achieved. This work develops a novel dual-state luminescent material, achieves persistent luminescence in both rigid and flexible matrices, and realizes efficient applications in oxygen and strain detection, flexible displays, 3D modeling, and complex dynamic information encryption, which will contribute to boosting practical and theoretical advancements of multifunctional long afterglow materials.

CRediT authorship contribution statement

Weirao Ji: Data curation, Investigation, Writing – original draft. Meiling Pan: Investigation, Software, Writing – original draft. Jinyu Duan: Investigation. Lei Ma: Software, Writing – review & editing. Yongtao Wang: Conceptualization, Funding acquisition, Supervision, Writing – review & editing.

Declaration of competing interest

The authors declare that they have no known competing financial interests or personal relationships that could have appeared to influence the work reported in this paper.

Acknowledgements

This work was supported by the National Natural Science Foundation of China (Grant No. 22565012) and the Guangxi Natural Science Foundation (Grant No. 2024GXNSFAA999457).

Appendix A. Supplementary data

Supplementary data to this article can be found online at https://doi.org/10.1016/j.talanta.2025.129058.

Data availability

No data was used for the research described in the article.

References

- S. Luo, X. Sun, L. Zhang, Y. Miao, G. Yan, Mn-doped ZnS quantum dots@dendritic mesoporous silica phosphorescent nanocomposites for antimicrobial susceptibility testing, Sensor. Actuat. B-Chem. 435 (2025) 137664, https://doi.org/10.1016/j. spb.2025.137664
- [2] S. Shen, X. Wang, Y. Li, Y.-e. Shi, Z. Wang, Room temperature phosphorescence-based sensor array for fluorescent brighteners through dehydration-induced doping, Sensor. Actuat. B-Chem. 427 (2025) 137244, https://doi.org/10.1016/j.snb.2025.137244
- [3] Q. Feng, Z. Xie, M. Zheng, Room temperature phosphorescent carbon dots for latent fingerprints detection and in vivo phosphorescence bioimaging, Sensor. Actuat. B-Chem. 351 (2022) 130976, https://doi.org/10.1016/j.snb.2021.130976.
- [4] R. Butkute, T. Serevicius, S. Raisys, K. Tulaite, L. Skhirtladze, G. Sini, J. V. Grazulevicius, S. Jursenas, Triplet harvesting in trifluoromethyl quinoxaline derivatives via TADF and RTP mechanisms, Opt. Mater. 158 (2025) 116421, https://doi.org/10.1016/j.optmat.2024.116421.
- [5] K. Chen, Y. Jiang, Y. Zhu, Y. Lei, W. Dai, M. Liu, Z. Cai, H. Wu, X. Huang, Y. Dong, Host to regulate the T₁–S₁ and T₁–S₀ processes of guest excitons in doped systems to control the TADF and RTP emissions, J. Mater. Chem. C 10 (32) (2022) 11607–11613, https://doi.org/10.1039/d2tc02167f.
- [6] Y. Xiong, J. Gong, J. Liu, D. Wang, H. Wu, Z. Zhao, M. Fang, Z. Li, D. Wang, B. Z. Tang, Achieving diversified emissive behaviors of AIE, TADF, RTP, dual-RTP and mechanoluminescence from simple organic molecules by positional isomerism, J. Mater. Chem. C 10 (27) (2022) 10009–10016, https://doi.org/10.1039/d2tc01857h
- [7] G. Liu, L. Yue, Y. Wang, S. Xue, Q. Sun, W. Yang, Serial novel N-phenylcarbazole derivatives with two-in-one introduction of bromine and polar groups as hosts for efficient RTP and white emission regulation, Chem. Eng. J. 498 (2024) 155171, https://doi.org/10.1016/j.cej.2024.155171.
- [8] M. Stanitska, D. Volyniuk, B. Minaev, H. Agren, J.V. Grazulevicius, Molecular design, synthesis, properties, and applications of organic triplet emitters exhibiting blue, green, red and white room-temperature phosphorescence, J. Mater. Chem. C 12 (8) (2024) 2662–2698, https://doi.org/10.1039/d3tc04514e.
- [9] L. Gu, X. Wang, M. Singh, H. Shi, H. Ma, Z. An, W. Huang, Organic room-temperature phosphorescent materials: from static to dynamic, J. Phys. Chem. Lett. 11 (15) (2020) 6191–6200, https://doi.org/10.1021/acs.jpclett.9b03363.
- [10] Z. Hassan, J. Lahann, S. Bräse, Cyclophanes as emerging materials from synthesis to functions, Adv. Funct. Mater. 34 (47) (2024) 2410027, https://doi. org/10.1002/adfm.202410027.
- [11] C. Yang, M. Pan, J. Han, R. Sheng, L. Ruan, L. Ma, Y. Wang, Constructing efficient organic room-temperature phosphorescent materials and converting luminescent characteristics via methyl groups and host matrixes, Dyes Pigments 242 (2025) 112982, https://doi.org/10.1016/j.dyepig.2025.112982.
- [12] Y. Zhu, H. Wu, M. Pan, L. Ma, Y. Wang, Achieving ultralong-lived flexible room-temperature phosphorescence, detection of strain and photostability, and high-level data encryption based on benzophenone derivatives, Chem. Eng. J. 519 (2025) 165087, https://doi.org/10.1016/j.cej.2025.165087.
- [13] J. Guo, Y. Zhao, L. Ma, Y. Wang, Ultra-long room temperature phosphorescence, intrinsic mechanisms and application based on host-guest doping systems, Chin. J. Struct. Chem. 43 (9) (2024) 100335, https://doi.org/10.1016/j.cjsc.2024.100335.
- [14] H. Wu, L. Shi, C. Yang, Y. Wang, X. Wang, L. Ma, Ultralong room-temperature phosphorescence of crystalline organic luminogens: excitation-dependence, chirality, and host-guest doping, Spectrochim. Acta 344 (2025) 126667, https:// doi.org/10.1016/j.saa.2025.126667.
- [15] Y. Zhu, M. Pan, W. Ji, L. Ma, Y. Wang, L. Ruan, Modulating room-temperature phosphorescence of D-r-A luminogens via methyl substitution, positional isomerism, and host-guest doping, Spectrochim. Acta 330 (2025) 125763, https://doi.org/10.1016/i.saa.2025.125763.
- [16] W. Ji, Y. Zhao, Y. Zhu, L. Ma, Y. Wang, High contrast crystalline, dynamic, and excitation dependent room temperature phosphorescence by tuning acceptor structures, Dyes Pigments 240 (2025) 112852, https://doi.org/10.1016/j. dyepig.2025.112852.

- [17] J. Jiang, J. Liu, C. Hu, Y. Wang, L. Ma, Construction and fine tuning of host-guest doping systems and the underlying mechanism of room temperature phosphorescence, Dyes Pigments 222 (2024), https://doi.org/10.1016/j. dyepig.2023.111931.
- [18] W. Ji, Y. Zhao, J. Guo, L. Ma, Y. Wang, Rapid construction and intrinsic mechanism of host-guest room temperature phosphorescence systems, Opt. Mater. 157 (2024) 116416, https://doi.org/10.1016/j.optmat.2024.116416.
- [19] J. Jiang, C. Hu, Y. Wang, L. Ma, J. Guo, Ultralong organic room-temperature phosphorescence, multiple stimulus responsiveness and high-level anticounterfeiting based on multifunctional carbazolyl imidazolopyridine, Mater. Today Chem. 30 (2023) 101548, https://doi.org/10.1016/j.mtchem.2023.101548.
- [20] Y. Hong, Y. Zhao, L. Ma, Y. Wang, Tuning triplet excitons and dynamic afterglow based on host-guest doping, Spectrochim. Acta 324 (2025) 124955, https://doi. org/10.1016/j.saa.2024.124955.
- [21] L. Kong, Y. Zhu, S. Sun, H. Li, J. Wu, F. Tao, L. Wang, G. Li, Tunable multicolor afterglow including white light emission from poly(acrylic acid)-based room temperature phosphorescence materials via phosphorescence FRET, Dyes Pigments 214 (2023) 111242, https://doi.org/10.1016/j.dyepig.2023.111242.
- [22] L. Kong, Y. Zhu, S. Sun, H. Li, S. Dong, F. Li, F. Tao, L. Wang, G. Li, Tunable ultralong multicolor and near-infrared emission from polyacrylic acid-based room temperature phosphorescence materials by FRET, Chem. Eng. J. 469 (2023) 143931, https://doi.org/10.1016/j.cej.2023.143931.
- [23] Y. Zhu, S. Sun, H. Li, L. Kong, Y. Xu, F. Tao, L. Wang, G. Li, Achieving color-tunable persistent afterglow from ultralong polyacrylamide-based room-temperature phosphorescence materials through phosphorescence Förster resonance energy transfer, Eur. Polym. J. 202 (2024) 112600, https://doi.org/10.1016/j. eurpolymi.2023.112600.
- [24] S. Sun, T. Li, Y. Zhu, G. Wang, F. Yin, F. Li, F. Tao, L. Wang, G. Li, Construction of starch-based room temperature phosphorescence materials with wide colortunable long afterglow and even persistent near-infrared luminescence via Förster resonance energy transfer, Int. J. Biol. Macromol. 284 (2025) 138175, https://doi. org/10.1016/j.ijbiomac.2024.138175.
- [25] S. Kuila, S.J. George, Phosphorescence energy transfer: ambient afterglow fluorescence from water-processable and purely organic dyes via delayed sensitization, Angew. Chem. Int. Ed. 59 (24) (2020) 9393–9397, https://doi.org/ 10.1002/anie.202002555.
- [26] X. Jiao, W. Zhang, J. Zhi, Y. Wang, M. Wang, Z. Liu, J. Li, Ultra-long organic RTP host–guest doped systems based on pure 4-(1H-imidazole-1-yl)methyl benzoate as versatile hosts, Mater. Chem. Front. 9 (7) (2025) 1166–1173, https://doi.org/ 10.1039/d4qm01037j.
- [27] W. Xie, W. Huang, J. Li, Z. He, G. Huang, B.S. Li, B.Z. Tang, Anti-Kasha triplet energy transfer and excitation wavelength dependent persistent luminescence from host-guest doping systems, Nat. Commun. 14 (1) (2023) 8098, https://doi.org/ 10.1038/s41467-023-43687-0.
- [28] J. Chen, J. Liu, L. Zeng, G. Dong, X. Guo, M. Sun, H. Liu, Y. Dong, C. Zhang, W. Li, Temperature-dependent reversible afterglow between green, orange, and red in dual-delay organic doped material, Adv. Opt. Mater. 12 (34) (2024) 2401660, https://doi.org/10.1002/adom.202401660
- [29] S. Han, Y. Li, Z. Wang, X. Li, G. Wang, Naphthyl substituted guest induce efficient room temperature phosphorescence by a triplet-triplet energy transfer mechanism, Dyes Pigments 228 (2024) 112243, https://doi.org/10.1016/j. dvepig.2024.112243.
- [30] A. Vinod Kumar, P. Pattanayak, A. Khapre, A. Nandi, P. Purkayastha, R. Chandrasekar, Capturing the interplay between TADF and RTP through mechanically flexible polymorphic optical waveguides, Angew. Chem. Int. Ed. 63 (40) (2024) e11054. https://doi.org/10.1002/anie.202411054.
- (40) (2024) e11054, https://doi.org/10.1002/anie.202411054.
 [31] C. Kant, A. Shukla, S.K.M. McGregor, S.-C. Lo, E.B. Namdas, M. Katiyar, Large area inkjet-printed OLED fabrication with solution-processed TADF ink, Nat. Commun. 14 (1) (2023) 7220, https://doi.org/10.1038/s41467-023-43014-7.
- [32] Y. Wang, Y.-e. Shi, S. Shen, Z. Wang, Confinement and heating promoted RTP of flumequine, oxolinic acid and levofloxacin on papers for their detection and discrimination, Sensor. Actuat. B-Chem. 419 (2024) 136394, https://doi.org/ 10.1016/j.snb.2024.136394.
- [33] J. Zhou, D. Liu, L. Li, M. Qi, G. Yin, T. Chen, Responsive organic room-temperature phosphorescence materials for spatial-time-resolved anti-counterfeiting, Chin. Chem. Lett. 35 (11) (2024) 109929, https://doi.org/10.1016/j.cclet.2024.109929.
- [34] J. Xue, X. Mao, X. Zhao, T. Xie, H. Hu, Z. Li, W. Gao, Nitrogen-doped carbon dots with excitation-dependent room temperature phosphorescence for multi-level anticounterfeiting applications, J. Lumin. 275 (2024) 120757, https://doi.org/ 10.1016/j.jlumin.2024.120757.
- [35] Y. Wu, X. Fang, J. Shi, W. Yao, W. Wu, Blue-to-green manipulation of carbon dots from fluorescence to ultralong room-temperature phosphorescence for high-level anti-counterfeiting, Chin. Chem. Lett. 32 (12) (2021) 3907–3910, https://doi.org/ 10.1016/j.cclet.2021.04.040.
- [36] P. Wu, Z. Lv, B. Lü, M. Li, Z. Yan, M. Chen, T. Zhao, G. Chen, J. Rao, F. Peng, Papermill waste derived bioplastic with Excitation- and time-dependent

- phosphorescence color for sustainable flexible anti-counterfeiting, Nano Lett. 25 (29) (2025) 11467–11474, https://doi.org/10.1021/acs.nanolett.5c02816.
- [37] Y. Si, Y. Zhao, W. Dai, S. Cui, P. Sun, J. Shi, B. Tong, Z. Cai, Y. Dong, Organic host-guest materials with bright red room-temperature phosphorescence for persistent bioimaging, Chin. J. Chem. 41 (13) (2023) 1575–1582, https://doi.org/10.1002/cioc.202200838
- [38] Y. Fan, S. Liu, M. Wu, L. Xiao, Y. Fan, M. Han, K. Chang, Y. Zhang, X. Zhen, Q. Li, Z. Li, Mobile phone flashlight-excited red afterglow bioimaging, Adv. Mater. 34 (18) (2022) 2201280, https://doi.org/10.1002/adma.202201280.
- [39] P.-R. Su, T. Wang, P.-P. Zhou, X.-X. Yang, X.-X. Feng, M.-N. Zhang, L.-J. Liang, Y. Tang, C.-H. Yan, Self-assembly-induced luminescence of Eu³⁺-complexes and application in bioimaging, Natl. Sci. Rev. 9 (1) (2022) nwab016, https://doi.org/10.1093/nsr/nwab016.
- [40] X. Yu, W. Liang, Q. Huang, W. Wu, J.J. Chruma, C. Yang, Room-temperature phosphorescent γ-cyclodextrin-cucurbit[6]uril-cowheeled [4]rotaxanes for specific sensing of tryptophan, Chem. Commun. 55 (21) (2019) 3156–3159, https://doi. org/10.1039/c9cc00097f.
- [41] T. Li, N. Zhang, S. Zhao, M. Liu, K. Zhang, C. Zhang, J. Shu, T.-F. Yi, Long-lived dynamic room temperature phosphorescent carbon dots for advanced sensing and bioimaging applications, Coord. Chem. Rev. 516 (2024) 215987, https://doi.org/ 10.1016/j.ccr.2024.215987.
- [42] W. Qin, J. Ma, Y. Zhou, Q. Hu, Y. Zhou, G. Liang, Simultaneous promotion of efficiency and lifetime of organic phosphorescence for self-referenced temperature sensing, Chem. Eng. J. 400 (2020) 125934, https://doi.org/10.1016/j. cei/2020/12534
- [43] Z. Chen, J. Shi, Y. Zhou, P. Zhang, G. Liang, Polymer microparticles with ultralong room-temperature phosphorescence for visual and quantitative detection of oxygen through phosphorescence image and lifetime analysis, Chin. Chem. Lett. 36 (5) (2025) 110629, https://doi.org/10.1016/j.cclet.2024.110629.
- [44] Z. Yang, J. Qian, S. Zhao, Y. Lv, Z. Feng, S. Wang, H. He, S.T. Zhang, H. Liu, B. Yang, Highly sensitive thianthrene covalent trimer room-temperature phosphorescent materials for low-concentration oxygen detection, Angew. Chem. Int. Ed. 64 (25) (2025) e202424669, https://doi.org/10.1002/anie.202424669.
- [45] S. Wang, H. Shu, X. Han, X. Wu, H. Tong, L. Wang, A highly efficient purely organic room-temperature phosphorescence film based on a selenium-containing emitter for sensitive oxygen detection, J. Mater. Chem. C 9 (31) (2021) 9907–9913, https://doi.org/10.1039/d1tc02324a.
- [46] W.-J. Guo, Y.-Z. Chen, C.-H. Tung, L.-Z. Wu, Ultralong room-temperature phosphorescence of silicon-based pure organic crystal for oxygen sensing, CCS Chem. 4 (3) (2022) 1007–1015, https://doi.org/10.31635/ ccschem.021.202100932.
- [47] H. Liu, G. Pan, Z. Yang, Y. Wen, X. Zhang, S.T. Zhang, W. Li, B. Yang, Dualemission of fluorescence and room-temperature phosphorescence for ratiometric and colorimetric oxygen sensing and detection based on dispersion of pure organic thianthrene dimer in polymer host, Adv. Opt. Mater. 10 (12) (2022) 2102814, https://doi.org/10.1002/adom.202102814.
- [48] F. Nie, B. Zhou, K.-Z. Wang, D. Yan, Highly tunable ultralong room-temperature phosphorescence from ionic supramolecular adhesives for multifunctional applications, Chem. Eng. J. 430 (2022) 133084, https://doi.org/10.1016/j. cei.2021.133084
- [49] X. Wang, R. Su, S. Luo, S. Han, N. Yu, X. Chen, L. Gan, J. Huang, Elastomeric intrinsic optical anti-counterfeiting with dual-color RTP from dual n→π* transition and enhanced intersystem crossing, Adv. Funct. Mater. (2025) e11543, https://doi. org/10.1002/adfm.202511543.
- [50] H. Zheng, P. Cao, Y. Wang, X. Lu, P. Wu, Ultralong room-temperature phosphorescence from boric acid, Angew. Chem. Int. Ed. 60 (17) (2021) 9500–9506, https://doi.org/10.1002/anie.202101923.
- [51] M. Li, K. Ling, H. Shi, N. Gan, L. Song, S. Cai, Z. Cheng, L. Gu, X. Wang, C. Ma, M. Gu, Q. Wu, L. Bian, M. Liu, Z. An, H. Ma, W. Huang, Prolonging ultralong organic phosphorescence lifetime to 2.5 s through confining rotation in molecular rotor, Adv. Opt. Mater. 7 (10) (2019) 1800820, https://doi.org/10.1002/advm.201800820
- [52] J. He, X. Jiang, F. Xu, C. Li, Z. Long, H. Chen, X. Hou, Low power, low temperature and atmospheric pressure plasma-induced polymerization: facile synthesis and crystal regulation of covalent organic frameworks, Angew. Chem. Int. Ed. 60 (18) (2021) 9984–9989, https://doi.org/10.1002/anie.202102051.
- [53] D. Li, Y. Yang, J. Yang, M. Fang, B.Z. Tang, Z. Li, Completely aqueous processable stimulus responsive organic room temperature phosphorescence materials with tunable afterglow color, Nat. Commun. 13 (1) (2022) 347, https://doi.org/ 10.1038/s41467-022-28011-6.
- [54] D. Li, Z. Liu, M. Fang, J. Yang, B.Z. Tang, Z. Li, Ultralong room-temperature phosphorescence with second-level lifetime in water based on cyclodextrin supramolecular assembly, ACS Nano 17 (13) (2023) 12895–12902, https://doi. org/10.1021/acsnano.3c04971.